

# $\beta$ -CaSiO<sub>3</sub> and colloidal n-SiO<sub>2</sub> based blended cement composites- their properties, regression analysis and micro-characterization studies

 N.A. Nair,  T.S. Viswanathan 

School of Civil Engineering, Vellore Institute of Technology, Vellore, (Tamil Nadu, India)  
: [viswanathan.ts@vit.ac.in](mailto:viswanathan.ts@vit.ac.in)

Received 26 September 2022  
Accepted 9 January 2023  
Available on line 11 April 2023

**ABSTRACT:** This paper examines the effect on mechanical properties such as compressive strength, flexural strength, and dynamic modulus of elasticity (DYE) of different proportions of wollastonite ( $\beta$ -CaSiO<sub>3</sub>) and colloidal nano-silica (n-SiO<sub>2</sub>) partially replacing cement. Durability indicators (water absorption, sorptivity and sulphate treatment test) were also examined to ascertain the quality of hardened paste mixes with respect to the control mix. The regression models were found for mechanical properties using different parameters from the results obtained, and statistical relations were established and validated. Regression analysis shows the significance of every parameter considered and model for the prediction of mechanical strengths. Finally, the results were substantiated by the microstructural characterization by FESEM.  $\beta$ -CaSiO<sub>3</sub> and colloidal n-SiO<sub>2</sub> replaced cement by 15%, and 1.5%-6% with an offset of 1.5%, respectively at low (0.25), medium (0.40) and high (0.55) water/binder (w/b) ratio. FESEM micrographs showed dense Calcium-silicate-hydrate (CSH) gel and stratlingite (CASH) was formed by blended cement paste mixes containing  $\beta$ -CaSiO<sub>3</sub> and n-SiO<sub>2</sub>. n-SiO<sub>2</sub> at 3% and CaSiO<sub>3</sub> at 15% replacements of cement (NS3 mix) was the optimum replacement level for the cement paste mix. Analysed regression model suggests that the models and parameters were found significant and can also be used for prediction (based on R<sup>2</sup> values and p-value).

**KEY WORDS:** Pozzolans; Regression analysis; Mechanical properties; Durability; FESEM.

**Citation/Citar como:** Nair, N.A.; Viswanathan, T.S. (2023)  $\beta$ -CaSiO<sub>3</sub> and colloidal n-SiO<sub>2</sub> based blended cement composites-their properties, regression analysis and micro-characterization studies. *Mater. Construcc.* 73 [350], e312. <https://doi.org/10.3989/mc.2023.304722>.

**RESUMEN:** *Compuestos de cemento combinados a base de  $\beta$ -CaSiO<sub>3</sub> y n-SiO<sub>2</sub> coloidal: propiedades, análisis de regresión y estudios de microcaracterización.* Este artículo examina el efecto sobre propiedades mecánicas como la resistencia a la compresión, la resistencia a la flexión y el módulo dinámico de elasticidad (DYE) de diferentes proporciones de wollastonita ( $\beta$ -CaSiO<sub>3</sub>) y nanosilíce coloidal (n-SiO<sub>2</sub>) que reemplazan parcialmente al cemento. También se examinaron indicadores de durabilidad (absorción de agua, sorción y prueba de tratamiento con sulfato) para determinar la calidad de las mezclas de pasta endurecida con respecto a la mezcla de control. Se encontraron los modelos de regresión para las propiedades mecánicas utilizando diferentes parámetros a partir de los resultados obtenidos, y se establecieron y validaron relaciones estadísticas. El análisis de regresión muestra la importancia de cada parámetro y modelo considerados para la predicción de las resistencias mecánicas. Finalmente, los resultados fueron corroborados mediante la caracterización microestructural realizada por FESEM. El  $\beta$ -CaSiO<sub>3</sub> y el n-SiO<sub>2</sub> coloidal reemplazaron al cemento en un 15 % y entre un 1.5 % y un 6 % con una compensación del 1.5 %, respectivamente, en relación peso/peso baja (0.25), media (0.40) y alta (0.55). Las micrografías FESEM mostraron un gel denso de calcio-silicato-hidrato (CSH) y la estratlingita (CASH) formada por mezclas de pasta de cemento combinadas que contenían  $\beta$ -CaSiO<sub>3</sub> y n-SiO<sub>2</sub>. Los reemplazos de n-SiO<sub>2</sub> al 3% y CaSiO<sub>3</sub> al 15% de cemento (mezcla NS3) fueron el nivel de reemplazo óptimo para la mezcla de pasta de cemento. El modelo de regresión analizado sugiere que los modelos y parámetros se encontraron significativos y también se pueden usar para la predicción (basado en los valores R<sup>2</sup> y el valor p).

**PALABRAS CLAVE:** Puzolana; Análisis de regresión; Propiedades mecánicas; Durabilidad; FESEM.

**Copyright:** ©2023 CSIC. This is an open-access article distributed under the terms of the Creative Commons Attribution 4.0 International (CC BY 4.0) License.

## 1. INTRODUCTION

Supplementary Cementitious Materials (SCM) when included in the cementitious matrix, affects many properties positively either due to the physical effect (very fine particles of SCM) or physicochemical effect (pozzolanic reaction of SCM) which leads to enhancement of cement matrix (1). SCM improves both the strength and durability properties of cementitious composites. SCM are cost-effective and sustainable. It has been observed that 15-20% substitution of cement can greatly reduce CO<sub>2</sub> emissions (2). Many mineral admixtures such as Fly ash, Ground granulated blast furnace slag, silica fume, metakaolin, wollastonite and more are being currently used as partial or total replacements for cement in building materials.

Wollastonite ( $\beta$ -CaSiO<sub>3</sub>) is white coloured and has an acicular structure, and fibrous in nature and pozzolanic (3-6). The main advantages of using colloidal n-SiO<sub>2</sub> are high volume to surface area (7, 8) and no harm to humans. The powdered form of n-SiO<sub>2</sub> gives better results than the colloidal form but is very harmful to human health (9). The colloidal n-SiO<sub>2</sub> also has excellent dispersion properties and can be distributed evenly throughout the mix if applied correctly. The n-SiO<sub>2</sub> is an exceptional replacement for cement, which can significantly enhance concrete's mechanical and durability properties. However, n-SiO<sub>2</sub> can only replace cement at significantly less replacement levels, i.e., up to 5% depending on particle size and surface area of n-SiO<sub>2</sub> particles (10, 11). Therefore, for higher replacement of cement, wollastonite ( $\beta$ -CaSiO<sub>3</sub>) was included, to observe their interactions at constant replacement of CaSiO<sub>3</sub> (15%) and different replacement of n-SiO<sub>2</sub> (1.5%-6%). Using n-SiO<sub>2</sub> also decreases the impact of concrete on ecology by ten times by increasing the structure's life to 500 years (12).

The global warming potential of CaSiO<sub>3</sub> replaced cement block has shown a tremendous amount of reduction in CO<sub>2</sub> sequestration than ordinary cement block (13). CaSiO<sub>3</sub> improved flexural strength, ductility, and flexural toughness at certain replacement levels (14-16). CaSiO<sub>3</sub> and silica fume combinations have demonstrated promising results on the mechanical properties of partially replaced cement paste and mortar (5). It improves early age micro-level cracking in ultra-high performance concrete (UHPC) (6). CaSiO<sub>3</sub> and fly ash concrete properties were studied and showed improved mechanical strength and durability at different curing ages and w/b ratios (3). Colloidal n-SiO<sub>2</sub> improves the mechanical strength of concrete by 15-20% (17). Researchers have found that the n-SiO<sub>2</sub> reduced the dormant phase of hydration period, salt ion permeation, and setting time of the concrete. n-SiO<sub>2</sub> also improved the mechanical and durability properties of cements blended with slag, bottom ash, fly ash, ceramic waste powder, and so on (18, 19). The reasons for improved performance after

addition of n-SiO<sub>2</sub> were accelerated hydration, higher production of CSH gel, and filling of voids (20-22).

This research assesses the potential of ternary blend of cement with CaSiO<sub>3</sub> and colloidal n-SiO<sub>2</sub> as a better replacement for ordinary portland cement. The primary purpose of this project was to replace cement at higher amount about 15-20%, with the help of CaSiO<sub>3</sub> and n-SiO<sub>2</sub> and evaluate its mechanical and durability properties at different curing ages and w/b ratios. The other purpose was to develop a regression model for mechanical properties to give statistical significance to the results and predictions. The microstructural characterization were carried out to support mechanisms claimed in results and discussions.

## 2. MATERIALS AND EXPERIMENTS

### 2.1. Raw materials

One of the material with Class C pozzolan compositions (23) is wollastonite (5). Colloidal n-SiO<sub>2</sub> was also added for enhancing the properties of cement matrix.  $\beta$ -CaSiO<sub>3</sub> used here has a CaO content of 46.8%, SiO<sub>2</sub> 45.8%, and Fe<sub>2</sub>O<sub>3</sub> content of 4.61%, with no traces of SO<sub>3</sub>, which confers with the class C pozzolana (5). Colloidal n-SiO<sub>2</sub> is 99.2% nano-scale SiO<sub>2</sub>. A total of 5 mixes were selected apart from the control mix. The mix design was carried out by the packing density method. The experiments were conducted on fresh and hardened paste mixes. The marsh cone test and mini-slump cone test determined the PCE (Polycarboxyl ether)-based superplasticizer dosage. The superplasticizer was obtained from Fosroc India Pvt Ltd. Cement was 53 grade by IS 12269 (24). Superplasticizers were added with respect to total weight of binder materials. CaSiO<sub>3</sub> was procured from Wolkem India Pvt Ltd. and Nanosilica from Nouryon India Pvt Ltd.  $\beta$ -CaSiO<sub>3</sub> is a triclinic acicular crystalline structure. It has a specific gravity of 2.9 and bulk density of 1.5 g/ml. The hardness in Moh's scale is 4.5. Melting point of  $\beta$ -CaSiO<sub>3</sub> is 1540°C, and co-efficient of expansion is  $6.5 \times 10^{-6}$ . Aspect ratios of the  $\beta$ -CaSiO<sub>3</sub> microfibrils has not been defined in this paper, yet with help of FESEM micrographs few dimensions have been found (Figure 9g).

The mix design of various mixes by weight is given in Table 1a, and oxides present in the raw materials are given in Table 1b. From the literature review, we concluded that the CaSiO<sub>3</sub> as a partial replacement to portland cement could be replaced at 15% with significant results. Also, the n-SiO<sub>2</sub> replaced up to 5% of OPC and showed excellent mechanical and durability properties.

CaSiO<sub>3</sub> and cement were premixed by hand until a uniform colour was obtained. The samples are machine mixed with the help of a machine mixer. The

**Table 1a.** Mix design for 125 cm<sup>3</sup> of sample(percentage of material by weight).

Mix Code		Cement	$\beta$ -CaSiO <sub>3</sub>	n-SiO <sub>2</sub>	Superplasticizer	Water
W0	0.25	100% (220.25 g)	0% (0 g)	0% (0 g)	0.375% (0.8259 g)	55.06 g
	0.4	100% (174.25 g)	0% (0 g)	0% (0 g)	0.11% (0.1916 g)	69.7 g
	0.55	100% (144.13 g)	0% (0 g)	0% (0 g)	0% (0 g)	72.27 g
W15	0.25	85% (186 g)	15% (29.15 g)	0% (0 g)	0.41% (0.8968 g)	54.68 g
	0.4	85% (147.38 g)	15% (25.94 g)	0% (0 g)	0.125% (0.2166 g)	69.33 g
	0.55	85% (122 g)	15% (21.47 g)	0% (0 g)	0% (0 g)	78.91 g
NS1.5	0.25	83.5% (179.63 g)	15% (32.27 g)	1.5% (3.23 g)	0.43% (0.925 g)	53.78 g
	0.4	83.5% (142.75 g)	15% (25.64 g)	1.5% (2.56 g)	0.14% (0.2393 g)	68.39 g
	0.55	83.5% (118.5 g)	15% (21.29 g)	1.5% (2.13 g)	0% (0 g)	78.09 g
NS3	0.25	82% (173.38 g)	15% (31.72 g)	3% (6.34 g)	0.5% (1.057 g)	52.86 g
	0.4	82% (138.38 g)	15% (25.31 g)	3% (5.06 g)	0.14% (0.2362 g)	67.5 g
	0.55	82% (115 g)	15% (21.04 g)	3% (4.21 g)	0% (0 g)	77.14 g
NS4.5	0.25	80.5% (167.5 g)	15% (31.21 g)	4.5% (9.36 g)	0.5% (1.04 g)	52.02 g
	0.4	80.5% (134 g)	15% (24.97 g)	4.5% (7.49 g)	0.16% (0.2663 g)	66.58 g
	0.55	80.5% (111.75 g)	15% (20.82 g)	4.5% (6.25 g)	0% (0 g)	76.35 g
NS6	0.25	79% (161.75 g)	15% (30.71 g)	6% (12.28 g)	0.52% (1.064 g)	51.18 g
	0.4	79% (129.88 g)	15% (24.66 g)	6% (9.86 g)	0.2% (0.3288 g)	65.76 g
	0.55	79% (108.5 g)	15% (20.6 g)	6% (8.24 g)	0% (0 g)	75.53 g

**Table 1b.** Oxides and ignition loss in raw materials.

Materials	SiO <sub>2</sub>	Al <sub>2</sub> O <sub>3</sub>	Fe <sub>2</sub> O <sub>3</sub>	CaO	SO <sub>3</sub>	Na <sub>2</sub> O	MnO	MgO	TiO <sub>2</sub>	K <sub>2</sub> O	P <sub>2</sub> O <sub>5</sub>	LOI
Cement	19.6	4.93	4.61	65.6	2.56	0.24	806 ppm	0.93	0.42	0.48	0.30	2.96
$\beta$ -CaSiO <sub>3</sub>	45.8	1.21	4.61	46.8	3.11	617 ppm	0.41	0.48	827 ppm	0.11	998 ppm	1.9
n-SiO <sub>2</sub>	99.2	0	0	0	0	0.2	0	0	0	0	0	-

mixing was done by ASTM C305 (25). For mixes with colloidal n-SiO<sub>2</sub>, the mixing time at high speed has been increased by 5 mins for proper dispersion of nanoparticles in the paste mix (26).

## 2.2. Experiment regime

### 2.2.1. Mechanical properties

Fresh properties: Mini slump cone test and marsh cone test has been conducted to determine the compatibility and effectiveness of superplasticizer in paste mixes. Mini slump cone test consists of a slump cone of dimension 19 mm top diameter and 38.1 mm bottom diameter with height of 57.2 mm. Plexi glass sheet was used for unhindered flow of paste mixes after lifting the mini cone. The paste mix of 200 ml is mixed and poured into the mini cone sitting over a

plexi glass sheet. The mini cone is lifted and the paste mix is allowed to spread over the plexi glass. The diameter of the spread is measured at 4 different places. The Marsh cone test was conducted in accordance with ASTM D6910. The paste's fluidity is inversely proportional to flow time of marsh cone. The marsh cone flow time is selected by plotting a log time vs superplasticizer dosage. A saturation point is reached in this graph when any increase in superplasticizer dosage does not significantly effect the fluidity of the paste mix (i.e. superplasticizer has no plasticizing effect). This saturation point is considered as the marsh cone flow time.

Compressive strength: Uniaxial compressive strength testing was carried out on 50 mm cube specimens. High-Performance paste cubes were cured and tested for ages 3, 7, 28, and 90 days. The cubes are exposed to the environment during the first 24 h after casting. Specimens after demoulding are kept in wa-

ter curing for a designated number of days. The compressive testing machine (CTM) was set at a 0.6 kN/s loading rate (27). Specimens were weighed and tested immediately after removing from the water, and also the three specimens were tested per curing day per mix. Water binder (w/b) ratios were 0.25, 0.40, and 0.55. The cement was replaced by  $\text{CaSiO}_3$  at 15% for all mixes and n- $\text{SiO}_2$  at 1.5%, 3%, 4.5%, and 6% levels. Section 4.1 analyses the experimental results obtained for compression test.

**Flexural strength:** Three-point loading test was conducted on flexural beam specimens (40mm x 40mm x 160mm) at the curing ages of 28 days and 90 days. The test was conducted by ASTM C78. Three specimens were tested per mix. Section 4.2 analyses the experimental results obtained for flexural strength test.

**Dynamic Modulus of Elasticity (DYE):** Two specimens for each mix were tested for the Ultra-sonic pulse velocity test. The specimen density was found prior, and then the transmission time, pulse velocity, and DYE were found with the help of the Pundit instrument. 2 transducers with 54 kHz frequency and diameter of about 30 mm was used on flexure specimens of size 40mm x 40mm x 160mm. Direct measurement was made for the specimen, and the specimen and probes were greased before measurement. The DYE test was conducted after 28 days and 90 days of curing. Section 4.3 analyses the experimental results obtained from UPV test.

### 2.2.2. Durability properties

**Water absorption:** This test was conducted as per ASTM C642. Two specimens were tested for each mix. The test was carried out after 7 days, 28 days, and 90 days of curing. The capillary forces exerted by continuous pore structure cause fluids (liquid and gaseous) to be sucked into the body of material; this phenomenon is called water absorption (28). The ingress of harmful environmental and chemical agents can be analyzed by measuring the water absorption rate. The water absorption test gives a volume of permeable pores, and this porosity should not be mistaken as actual porosity.

**Sorptivity:** Sorptivity test was conducted as per ASTM C1585 (29). The specimens were cast, and after curing, the specimens were heated at 105°C for 24 h. The test was carried out for eight days. Water transport in concrete primarily happens in the pore system of hardened cement paste (30). Sorptivity consists of 2 stages: rapid primary absorption and slow secondary absorption. The graph of absorption rate vs. square root of time gives the coefficient of primary and secondary absorption. Sorptivity is also temperature dependent, especially primary absorption; therefore, care should be taken to keep the temperature constant, at least on day 1.

**Sulphate treatment test:** The sulphate treatment test was conducted on a 50 mm cube specimen after 28 days of water curing, for 28 days and for 90

days of sulphate solution immersion. The sodium sulphate solution prepared was a saturated solution. The saturated solution was changed every two weeks to maintain the fully saturated condition. Here, sulphate treatment's physical and chemical aspects will be studied. The term sulphate attack was not used here as there was no significant damage found in the paste mixes, as suggested by A. Neville (31). The reaction of environmental sulphates with hydrated phases of cement paste forms ettringite, gypsum, or both at any temperature (31, 32). A sulphate attack can be broadly classified as a physical sulphate attack, and a chemical sulphate attack wherein the sodium sulphate salt crystallization happens during a physical sulphate attack (33). The most plausible mechanism of sulphate attack expansion was crystallization and swelling pressure created by the ettringite crystals (34, 35). Firstly, gypsum was formed by calcium hydroxide dissolution and increased penetration of external sulphate solution, and later ettringite is formed by gypsum reacting with calcium aluminates hydrate (36).

### 2.2.3. Microstructure study

**Field Emission Scanning Electron Microscopy (FESEM):** Thermo Fisher FEI QUANTA 250 FEG was used to study the surface morphology of the paste mixes with help of micrographs. The operating voltage ranges from 5kV to as high as 30kV. It also offers a high resolution of 1.2 nm under high vacuum conditions at high voltages. The FESEM micrograph analysis combined with Energy-dispersive X-ray spectrometer (EDS) gives the compositional analysis of the paste mix. The samples are to be gold coated before viewing under an electron microscope as the paste sample was a non-reflective surface. FESEM used is shown in Figure 1. FESEM was conducted on powdered samples collected from broken samples. The samples for microstructural study was dipped for 10 days in 99% isopropyl alcohol for solvent exchange method. After 10 days, the sample are heated to 105° C for 24 h in hot air oven for solvent removal. The samples are then kept in air tight containers till the date of imaging. The samples are coated with gold before loading to sample holder. The samples were tested for 28 days and 90 days. 36 samples from cube and flexure specimens, and 6 samples from the edges of specimens after the sulphate treatment test was conducted.

## 3. RESULT AND DISCUSSIONS

### 3.1. Fresh properties

Table 2 shows the mini slump cone test and marsh cone flow time values. The optimum superplasticizer dosage for all paste mixes for 0.25 and 0.4 w/b ratios were determined. The wollastonite microfibres and



FIGURE 1. Thermo Fisher FEI Quanta 250 FEG.

nanosilica decreases the fluidity of the paste mix and hence demands more superplasticizer dosage than the reference mix.

### 3.2. Compressive strength

Figure 2 shows that the reinforcement effect of CaSiO<sub>3</sub> and colloidal n-SiO<sub>2</sub> was significant even

though the compressive strength was lower than the control mix—CaSiO<sub>3</sub> and colloidal n-SiO<sub>2</sub> show better strength at 28 days, representing their reinforcement effect. After 28 days, mix NS3 shows the highest strength at 0.25 and 0.40 w/b ratios. It suggests a high secondary reaction by CaSiO<sub>3</sub> and colloidal n-SiO<sub>2</sub>.

The secondary reaction will reduce the amount of ettringite and calcium hydroxide and increase the dense CSH gel (5, 22, 26, 37). The strength development can also be attributed to matrix densification and pore size refinement. Strength improved with a decrease in w/b ratios; the highest compressive strength was observed in the 0.25 w/b ratio and the lowest in the 0.55 w/b ratio. Free water, available for reaction, reacts with the cement, CaSiO<sub>3</sub>, and colloidal n-SiO<sub>2</sub> to form different hydrates responsible for strength development. The excess water goes and settles in different pores and evaporates after some time, leaving voids in the paste matrix. It results in the weakening of the paste matrix (38). The increase of nano silica after 3% causes a reduction in strength, which can be attributed to the amount of n-SiO<sub>2</sub> particles greater than the amount of free lime in the hydration process. It results in excess silica leaching; hence, the n-SiO<sub>2</sub> acts as a pore filler and does not take part in the hydration process at this point (22, 39). Figure 3 shows the parallel cracks inclined at a slight angle to the applied load, formed in the specimen suggests axial compression caused due to localised tensile stress acting normal to the applied load. The cracks formed are shown in Figure 3a and 3b. In Figure 3c, CaSiO<sub>3</sub> and n-SiO<sub>2</sub> provide reinforcement to the hardened cement matrix, which hinders the crack propagation as described by Neville (40).

Initially, the paste mix was wet; hence the CaSiO<sub>3</sub> and colloidal n-SiO<sub>2</sub> reaches the voids by passing through the pore solution in the paste mix. This mechanism helps the SCMs to have secondary hydration reactions in the future, thereby forming CSH gel and reducing the number of capillary pores. The rate of secondary hydration varies with respect to the chemical and physical properties of admixtures, and also the fill-

TABLE 2. Fresh properties.

Sl. No.	Mix Designation	Optimum Superplasticizer (SP) dosage (%)		Average flow (cm)		Average Flow/SP dosage		Marsh cone flow time (log s)	
		0.25	0.4	0.25	0.4	0.25	0.4	0.25	0.4
1	W0	0.375	0.11	15.625	15.575	41.667	141.591	2.3329432	2.137772
2	W15	0.41	0.125	15.25	15.375	37.195	123.000	2.1891533	1.983707
3	NS1.5	0.43	0.14	15.25	15.25	35.465	108.929	1.9915805	1.849911
4	NS3	0.5	0.14	15.475	15.2	30.950	108.571	1.9378187	1.837336
5	NS4.5	0.5	0.16	15.1	15.2	30.200	95.000	1.9139198	1.795463
6	NS6	0.52	0.2	15.325	15.7	29.471	78.500	1.9059038	1.603577

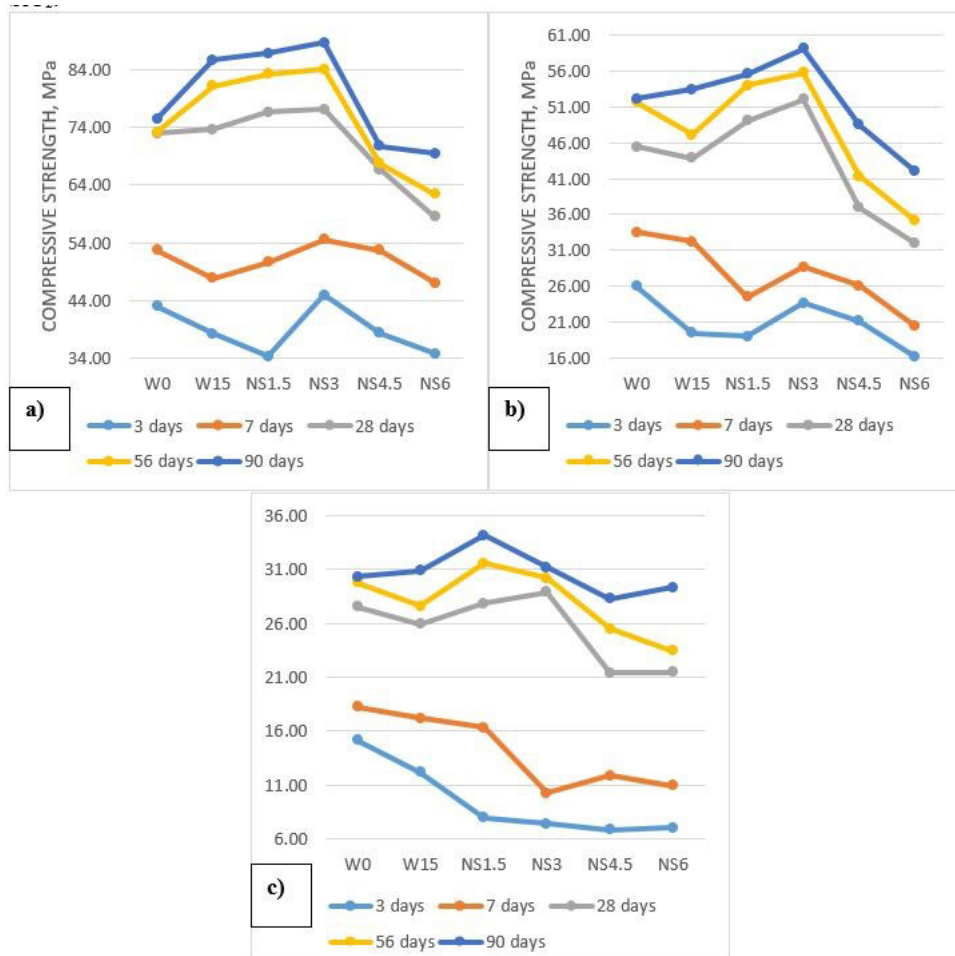


FIGURE 2. Compressive strength of paste mixes a) 0.25 w/b, b) 0.40 w/b, and c) 0.55 w/b.

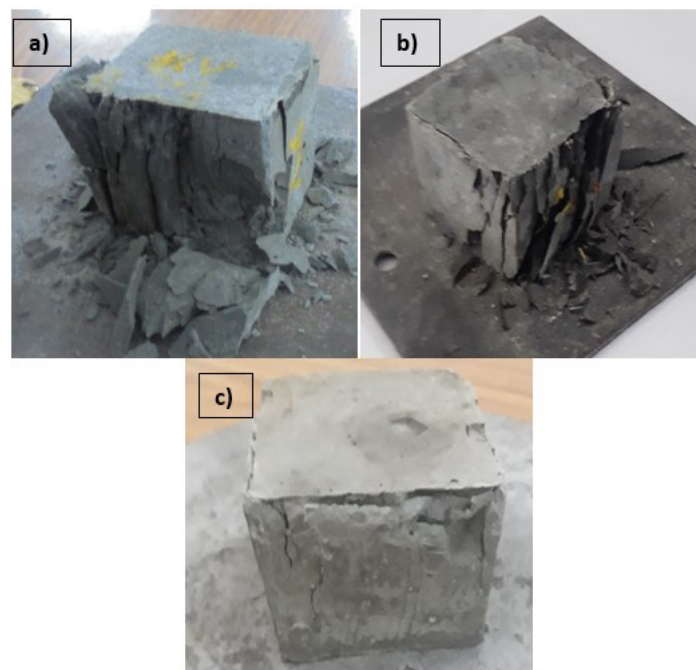


FIGURE 3. Cracked specimens under axial compressive load: a) and b) cracks formed in control specimen, c) cracks formed in NS3 specimen.

er effect increases the compressive strength of the paste matrix. When using an admixture, it was favourable if improvement by filling voids and secondary hydration was more significant than the strength development imparted by the control mix at all ages of curing (41). The n-SiO<sub>2</sub>, along with CaSiO<sub>3</sub>, gives a collabrated effect of secondary hydration and reinforcement, making them an early age strength developer.

### 3.3. Flexural strength

Flexural strength depends more on binding between the various particles than the density of the paste mix (11). Therefore, wollastonite's reinforcement and colloidal n-SiO<sub>2</sub> strong pozzolanic action will have more effect than pozzolanicity of CaSiO<sub>3</sub> alone.

The flexural strength at 3% n-SiO<sub>2</sub> replacement shows the highest values of flexure at 28 days, as seen in Figure 4. The n-SiO<sub>2</sub> will fill the cement pores, thereby increasing the flexural strength. Nanosilica contributes to flexural strength by producing more CSH gel by reacting with CH (22, 42). The CaSiO<sub>3</sub>

reinforces the paste matrix and thus shows better results than the control mix, about 54.4%\* (0.25 w/b ratio) and 55.3% (0.40 w/b ratio) at 28 days of curing. At 90 days, NS3 showed the highest flexural strength at both 0.25 w/b ratio (29.77%\*) and 0.40 w/b ratio (43.2%\*). At higher replacement levels of n-SiO<sub>2</sub>, the flexural strength decreased, and the increase in flexural strength at 0.25 w/b ratio than 0.40 w/b ratio at all ages was the same as discussed above. “\*” indicates the percentage change with respect to control mix.

### 3.4. Dynamic Modulus of Elasticity (DYE)

DYE can be determined from the UPV test when the specimen's density was known. DYE of 0.25 w/b ratio and 0.40 w/b ratio was determined for 28 and 90 days and plotted as a graph in Figure 5. The highest DYE value and transmission time value was observed in NS3 at all w/b ratio and all curing ages. NS3 shows 40% and 58% improvement in DYE to the control mix at 0.25 and 0.40 w/b ratios, respectively. DYE increase can be associated with an increase in the den-



FIGURE 4. Flexural strength of paste mixes.

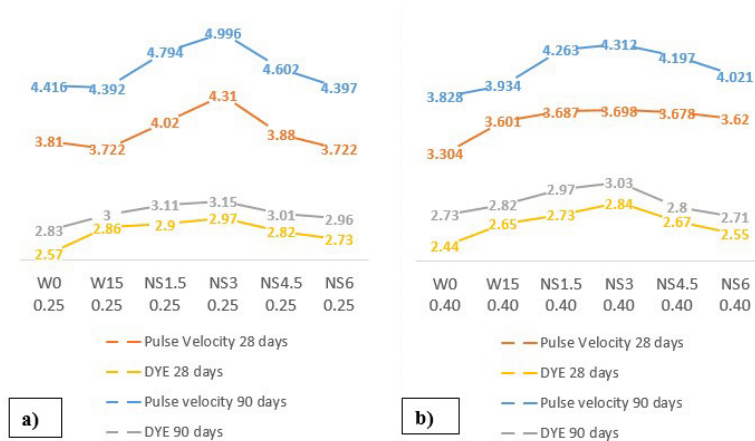


FIGURE 5. Dynamic Young's modulus of Elasticity (DYE) a) 0.25 w/b, b) 0.40 w/b.

sity of the matrix. The increase can also be explained by the reinforcing effect of CaSiO<sub>3</sub> microfibrils which acts as a bridge for microcracks (6). The reduction of porosity in the matrix enhances the DYE, shown in the water absorption experiment. DYE was measured in GPA, whereas pulse velocity was measured in km/s.

### 3.5. Regression analysis of mechanical properties

In this study, we need predictive models from the experimental output. Therefore, we have used regression analysis. The residual plot shown in Figure 6 indicates that the models are sufficient and do not infringe the three assumptions of the ANOVA test (43).

The results obtained from the experiments conducted on the specimens were fitted into a linear regression model to develop mathematical relations between mechanical properties and various parameters. We recommend that Equation [1] be used as a regression model, as it incorporates all continuous variables or parameters. The parameters which affect the compressive strength, flexural strength, and DYE are w/b ratios, curing age, amount of n-SiO<sub>2</sub>, and Ca-SiO<sub>3</sub> (44, 45).

Different parameters can affect the properties of individuals or together in combinations. Variance inflation factor (VIF) can help us find the existence of multicollinearity in the model obtained. While equations have good fit and correlations, the models must be constantly updated to accurately quantify these mechanical properties (46, 47).

$$\text{Response} = \sum_{i=0}^n \beta_i x_i + \text{Error} \quad [1]$$

Where,  $x_i$  – variables or parameters,  
 $\beta_i$  – coefficients of the parameters,  
 $\beta_0$  – constant term,

Response- mechanical properties.

The ANOVA model identified significant parameters, and interactions between parameters and response variables were studied.

Equation [2] shows the regression model between compressive strength and other parameters. The least square method was used to find the coefficients of the model. P-value was considered to find the significant ( $p \leq 0.05$ ) and insignificant ( $p > 0.05$ ) parameters. The statistically insignificant parameters can be omitted from the final Equation [2] (45).

$$f_c = 114.6 - 185.9 w/b + 0.1349 \text{ age} - 2.57 \text{ Nanosilica} + 0.461 \text{ Wollastonite} \quad [2]$$

Where,  $f_c$  – Compressive strength

Similarly, flexural strength and DYE were statistically analysed with identical parameters, and the following equations were found.

$$\sigma = 2.847 - 5.55 w/b + 0.03912 \text{ age} - 0.1414 \text{ Nanosilica} + 0.1455 \text{ Wollastonite} \quad [3]$$

Where,  $\sigma$  – Flexural strength

$$\delta = 2.808 - 1.094 w/b + 0.03212 \text{ age} - 0.01950 \text{ Nanosilica} + 0.01867 \text{ Wollastonite} \quad [4]$$

Where,  $\delta$  – DYE.

#### 3.5.1. Analysis of variance (ANOVA):

ANOVA was performed on the linear regression model to find the significance of the model and the influence of each parameter on the response variable or individual mechanical property. The F-value and p-value related to the models suggest that these models give a better fit than the model with all dependent factors. Thus, we can infer that the response variable is related to at least one factor. In table 3, we can see the model summary suggesting the models obtained here are statistically significant. The slight difference between R<sup>2</sup> and R<sup>2</sup> (adjusted) values shows that these models have not included an insignificant term. The compressive and flexural strength models' R<sup>2</sup> values indicate that they are significant statistically and can predict these properties for new experiments conducted within these parameters boundary limits. Even though the R<sup>2</sup> value of DYE is statistically significant, the prediction of DYE values will give many observations with high SD and coefficient of variation. Hence, it is not advised to refer to the DYE equation obtained in this study. A separate model of DYE can be prepared with reduced autocorrelation as discussed in the Durbin-Watson statistic test.

The standard deviation of the model is low as the coefficient of variation is less than 1. The distribution of values is mainly centered near to mean.

#### 3.5.2. Durbin-Watson statistic:

Regression output has to check for autocorrelation, which the Durbin-Watson statistics test can do. This statistic value ranges from 0-4. Furthermore, a value near 2 confirms zero correlation. There is no autocorrelation for compressive and flexural strength as the Durbin Watson stat value is near 2, but for DYE, there is some positive autocorrelation, as shown in Table 3.

Table 4 shows that all the parameters are significant, with a p-value less than 0.05 and high F-value. It infers that the main effect of the four parameters is statistically significant.

The main effect of w/b suggests that as the w/b increases, all mechanical properties decrease. It can be attributed to the presence of voids increasing the

TABLE 3. Model Summary.

S	R <sup>2</sup>	R <sup>2</sup> (adjusted)	R <sup>2</sup> (predicted)	Durbin-Watson Statistic
Compressive strength				
5.11497	91.96%	90.26%	87.73%	2.00506
Flexural strength				
0.602132	88.21%	85.73%	81.82%	1.96766
DYE				
0.088265	80.14%	75.96%	69.57%	1.88245

TABLE 4. Parameters significance.

Sl. No.	Parameters	Compressive strength		Flexural strength		DYE	
		F-value	p-value	F-value	p-value	F-value	p-value
1	W/B	178.37	0.000	11.48	0.003	20.76	0.000
2	Age	16.05	0.001	97.35	0.000	30.55	0.000
3	Nanosilica	22.72	0.000	4.96	0.038	4.39	0.050
4	Wollastonite	4.57	0.046	32.84	0.000	25.16	0.000

porosity and thereby decreasing the density of the matrix (48). The presence of CaSiO<sub>3</sub> and n-SiO<sub>2</sub> can also explain the increase in mechanical properties of the control mix. CaSiO<sub>3</sub> is ductile due to its fibrous nature, and n-SiO<sub>2</sub> forms a dense matrix by forming more CSH gel. These compounds have mechanisms such as diversion of cracks, filling of pores, and delay in cracking, which makes the cement matrix have improved mechanical properties. Mechanical properties also increase with curing age as the CaSiO<sub>3</sub> is a weak pozzolan and can form hydration products later, making the cement matrix dense and less porous.

### 3.6. Water absorption

Different parameters were found according to ASTM C642, and the data was tabulated and analysed (49). Figure 7 shows the percentages of the volume of permeable pores, absorption after immersion, and absorption after boiling for various mixes. The NS3 mix showed the lowest values at 0.25 w/b ratio 28 days result.

Figure 7 shows the least volume of permeable pores and, subsequently, the most negligible water absorption among the paste mixes. At 28 days, a 0.25 w/b ratio of 3% n-SiO<sub>2</sub> and 15% CaSiO<sub>3</sub> (NS3) replacement has almost 20.9% less permeable pores than the control mix. Similarly, for a 0.40 w/b ratio, the difference is 18%, and for a 0.55 w/b ratio, the

difference is 18%. At all ages and w/b ratios, NS3 has shown better results than any other paste mixes. At 90 days, 0.25 w/b ratio NS3 has almost 35% less porosity than the control mix, in 0.40 w/b ratio, porosity is reduced by 33% than the control mix, and in 0.55 w/b ratio porosity decreases by 30% than the control mix. Adding CaSiO<sub>3</sub> alone (W15) increases the volume of permeable pores, thereby increasing water absorption. The increase in permeable pores is significantly less in a low w/b ratio, suggesting a reduction in capillary pores and densification compared to higher w/b ratios (1, 50). High n-SiO<sub>2</sub> replacements NS4.5, and NS6 showed better water absorption and volume of pores than the control mix and W15 mix, suggesting that the permeable pores reduce and water absorption through the paste mix also reduce. This can be explained by presence of unreacted n-SiO<sub>2</sub> in the voids as shown in micrographs (Figure 9a), thereby, densifying the blended cement matrix. A higher w/b ratio means higher initial porosity for the voids to be filled by hydrates. Superplasticizers give better compaction to the powder and result in a better hydration reaction as it deflocculates the cement and SCMs (51).

### 3.7. Sorptivity

Figure 8 shows the sorptivity values at 28 days and 90 days. The absorption within the first 6 h, i.e.,

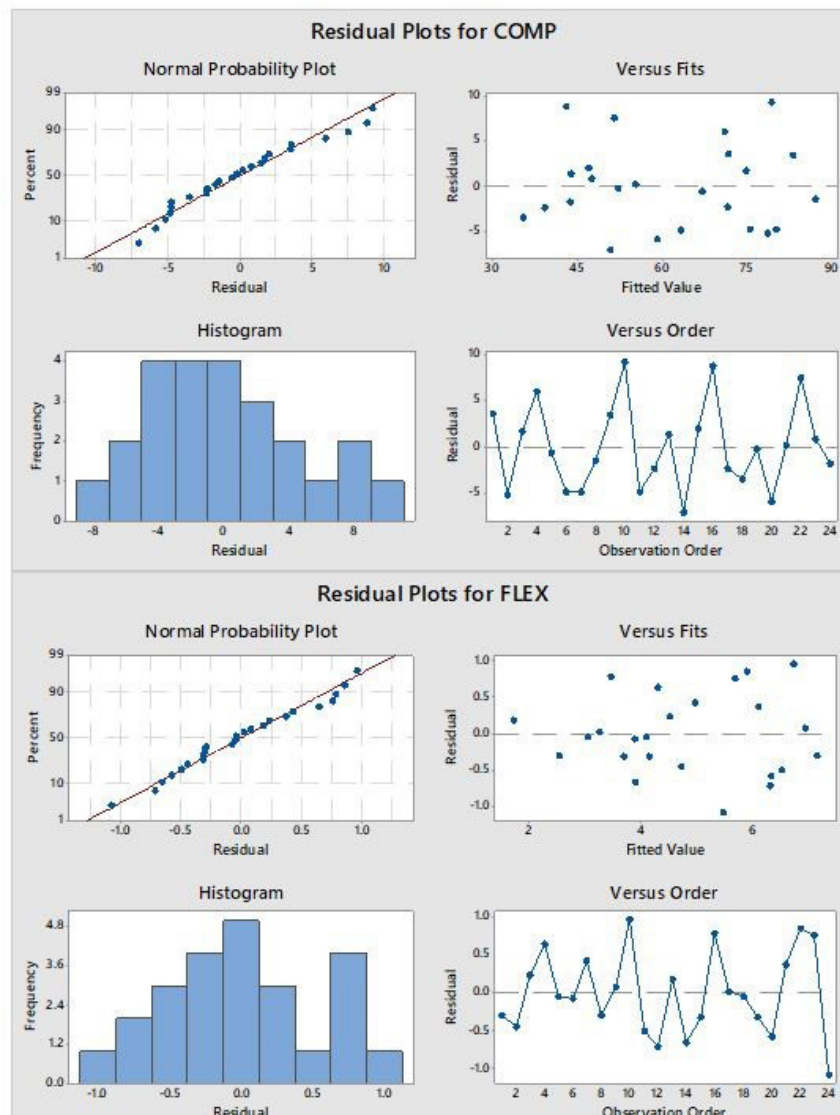


FIGURE 6. Residual plots.

initial sorptivity has the maximum ingress of water and after which the secondary sorptivity happens till 8 days. Here, it can be observed that the sorptivity value increases with the w/b ratio and decreases as curing age increases. At 0.25 w/b ratio, the initial sorptivity and secondary sorptivity is very low compared to 0.40 w/b and 0.55 w/b ratios. This is due to very low porosity at 0.25 w/b ratio. Control mix has the highest sorptivity whereas, the NS3 mix has the lowest sorptivity. The n-SiO<sub>2</sub> present in the mix blocks the pores of present in the matrix and effectively blocks the interconnectivity of the pore network (52). The lowest sorptivity values can be seen in NS3 in all w/b (0.25, 0.40, 0.55) and all curing ages (28 and 90 days). The sorptivity generally happens due to capillary pores present in the cement paste matrix. The capillary suction by interconnected pores is the least in the NS3 mix due

to matrix densification and pore discontinuity due to mineral admixtures added. At a low w/b ratio, the superplasticizers help in dispersing the n-SiO<sub>2</sub> and CaSiO<sub>3</sub> to the pores and act as fillers, and form hydrates after primary and secondary reactions (3, 5, 22, 39, 42). The highest sorptivity values were found in NS6 and control paste mixes at different curing ages and w/b ratios. This can be explained by high capillary pores present in these mixes enabling transport of water through the paste matrix.

From table 5, we have found the values of permeable pore radius with help of Hagen-Poiseuille formula and Lucas-Washburn model (53). A relationship between pore radius, sorptivity, and porosity which is as follows:

$$P_r = \frac{1}{c} \left( \frac{l}{\omega} \right)^2 \quad [5]$$

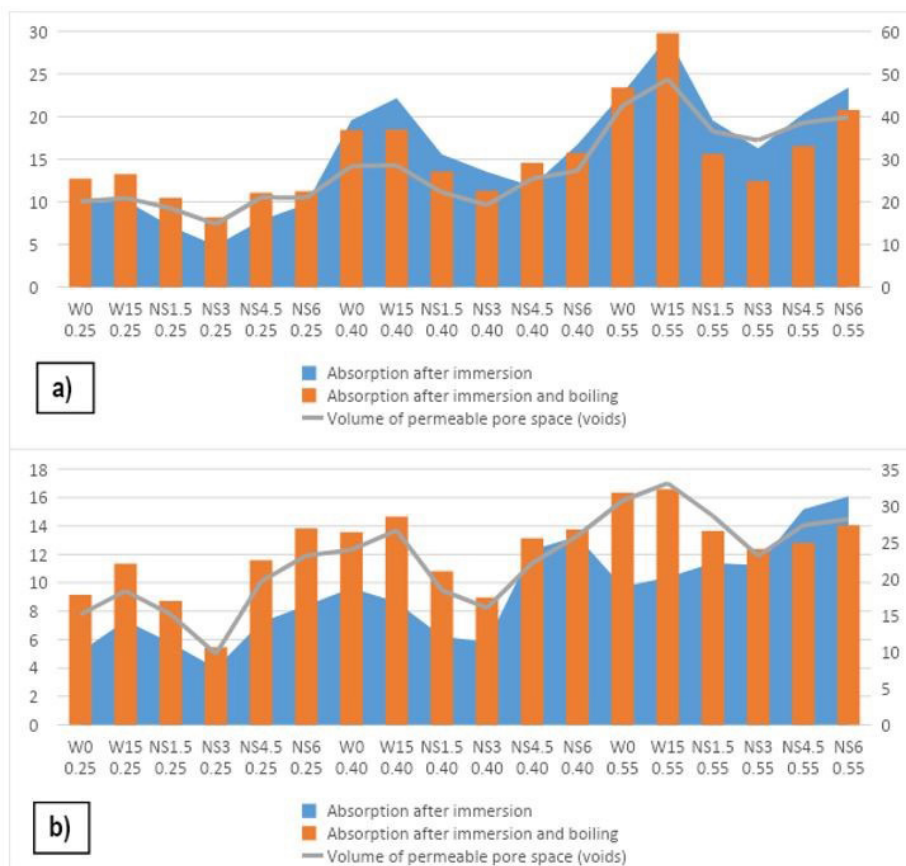


FIGURE 7. Water absorption a) 28 days, b) 90 days.

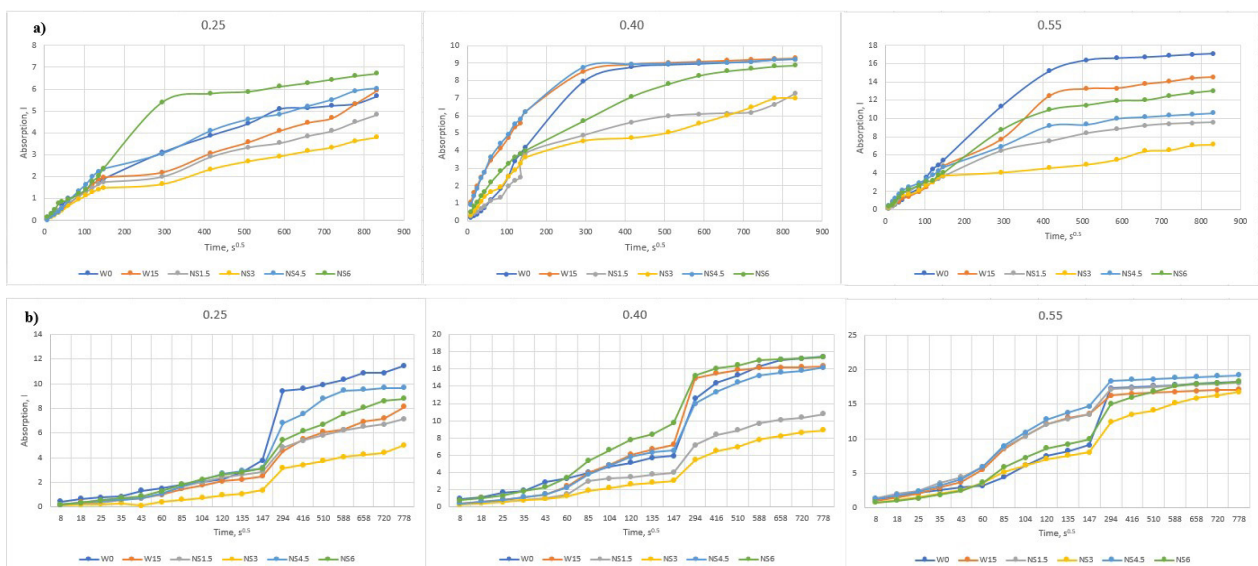


FIGURE 8. Sorptivity values a) 28 days, b) 90 days.

Where,  $C = \text{constant} = (\gamma \cos \Theta / 2\eta)$ ,  $\gamma$ - surface tension of water,  $\Theta$ - contact angle of water,  $\eta$ - dynamic viscosity of the liquid,  $\omega$  - porosity,  $I$ -sorptivity.

As suggested earlier, the pore radius increases as the w/b ratio increases. The pore radius is minimum

in NS3 at all w/b ratios, and curing ages and the pore radius is maximum for NS6 and control mix. These results corroborate with the mechanical and durability properties.

TABLE 5. Pore radius calculations.

Sl. No.	Mix Designation	0.25		0.4		0.55	
		28 days	90 days	28 days	90 days	28 days	90 days
1	W0	1.19455E-08	1.05285E-08	1.21147E-07	1.14753E-07	4.43033E-07	3.76854E-07
2	W15	1.26687E-08	3.17302E-09	1.20774E-07	1.1743E-07	4.18904E-07	3.69151E-07
3	NS1.5	8.06896E-09	7.56676E-09	1.26288E-07	8.14237E-08	3.86653E-07	3.1677E-07
4	NS3	4.30676E-09	1.79341E-10	1.20881E-07	8.88839E-08	4.24036E-07	3.30997E-07
5	NS4.5	1.69429E-08	3.65832E-10	1.24352E-07	1.1472E-07	3.8364E-07	3.09135E-07
6	NS6	1.13675E-08	6.55556E-11	1.13076E-07	1.05667E-07	3.73158E-07	3.14485E-07

### 3.8. Sulphate treatment test

Table 6 shows that at a 0.25 w/b ratio, the paste mix NS3 has the lowest change in compressive strength and mass compared to other mixes. It signifies that the NS3 mix at 0.25 w/b has a dense matrix with low capillary pores, which does not permit the ingress of a harmful chemical such as sodium sulphate, thereby increasing the durability of structures. However, table 6 has different paste mixes representing the lowest values, i.e., NS1.5. The change in optimum value is

due to an increase in water content; the higher water content increases the porosity, increasing the ingress of harmful chemicals. In table 6, the optimum found at a 0.55 w/b ratio is NS4.5. The increased n-SiO<sub>2</sub> at higher water content resulted in the formation of hydrates at pores. It resulted in an increased density of the matrix and a reduction in the ingress of harmful solutions (5, 22, 37).

After 90 days curing, loss of compressive strength and mass was observed in high w/b ratios of 0.40 and 0.55. Hence, we can characterize these as sulphate

TABLE 6. Sulphate treatment test.

Sl. No.	Mix Designation and w/b	Change in Mass ( $\Delta m$ )		Compressive strength, After Sulphate treatment (difference from normal samples)		
		28 d	90 d	28 d	90 d	
1	W0	0.25	2.85	3.3	76.2 (3.21)	76.6 (-2.87)
		0.4	16.4	-2.85	53.2 (7.77)	46.4 (-5.77)
		0.55	20.5	-5.45	32.4 (4.87)	23.8 (-6.55)
2	W15	0.25	2.4	3.45	74.5 (0.87)	81.2 (-4.53)
		0.4	16.8	-2.85	47.9 (4.07)	48.4 (-4)
		0.55	21.25	-5.8	30.8 (4.86)	24.2 (-6.7)
3	NS1.5	0.25	0.75	1	77 (0.33)	84.6 (-2.2)
		0.4	15.45	-1.35	51.1 (2)	54.8 (-0.8)
		0.55	17.2	-2.4	30.8 (2.92)	30.6 (-3.24)
4	NS3	0.25	0.7	0.8	77.20 (0.13)	87.8 (-0.87)
		0.4	15.7	-1.45	54.9 (2.87)	57 (-2.07)
		0.55	18.3	-2.6	32.2 (3.29)	30.6 (-0.62)
5	NS4.5	0.25	2.8	3.9	67.68 (1)	67 (-3.8)
		0.4	16.75	-2	41.1 (4)	45.4 (-3.13)
		0.55	22.45	-0.45	24 (2.57)	26 (-2.31)
6	NS6	0.25	3.25	4.2	58.8 (0.27)	65 (-4.47)
		0.4	16.95	-2.4	35.6 (4.8)	34.6 (-5.53)
		0.55	22.65	-3.3	25.4 (3.94)	20.4 (-8.94)

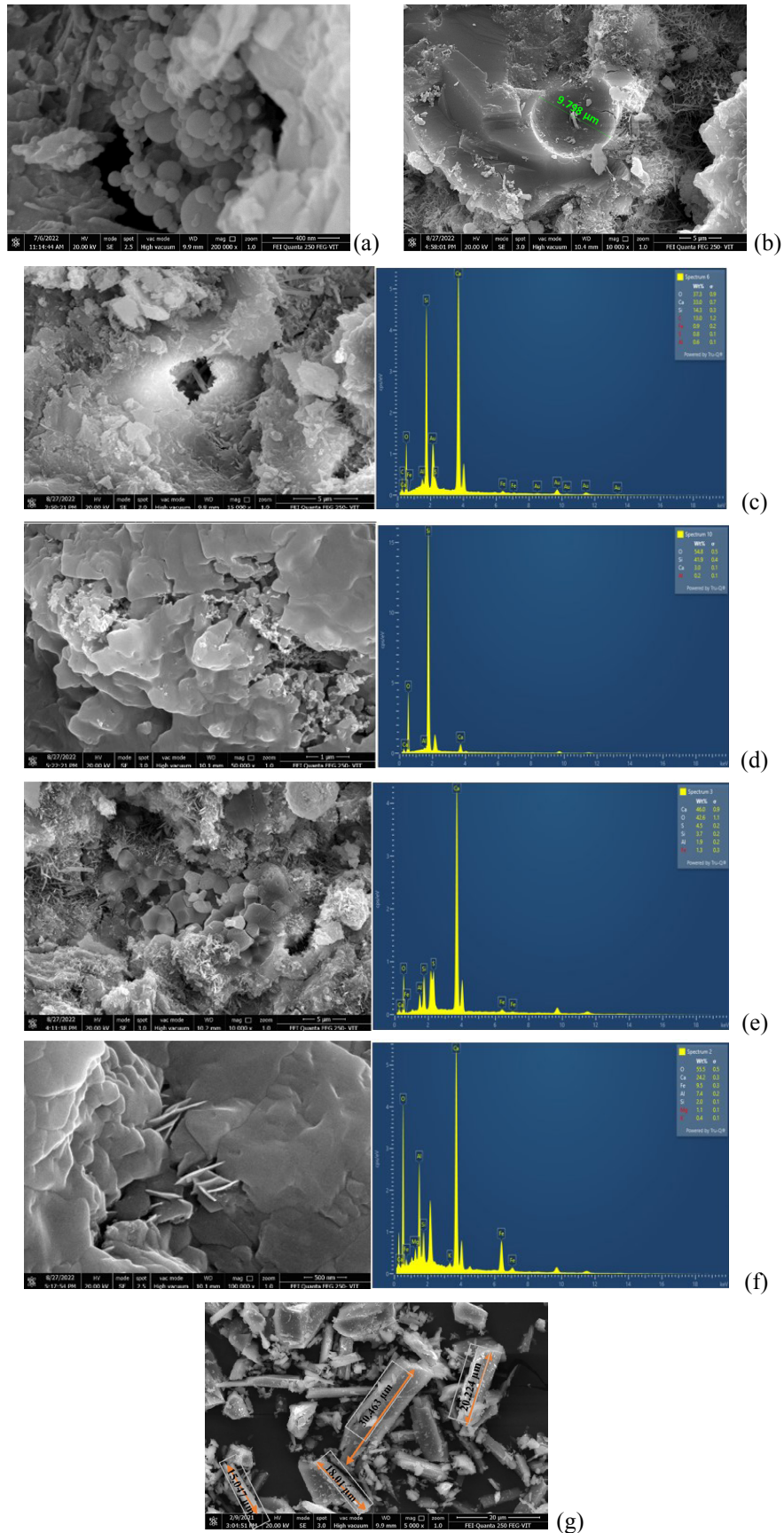


**FIGURE 9.** FESEM images and EDS of paste matrix a) Unreacted n-SiO<sub>2</sub>, b) Pores in paste matrix, c) Voids filled by CaSiO<sub>3</sub>, d) Voids filled by n-SiO<sub>2</sub>, e) Calcium oxide and ettringite present in control mix, f) Stratlingite presence in voids of blended cement paste matrix, g) Wolastonite particle sizes.

attacks (31). At 28 days and a 0.25 w/b ratio, there was no significant change in compressive strength or mass. At 28 days and 0.40 w/b ratio and 0.55 w/b ratio, there is an increase in compressive strength and mass. It suggests that the sodium sulphate solution at 28 days has no significant or negative effect on the paste mixes at 28 days. Thus, there is no need to conduct experiments for the sulphate treatment test at 28 days. However, at 90 days, we can see sodium sulphate attacking the paste mix. Though the decrease is significantly smaller in the 0.25 w/b ratio, the increase is significantly higher at the 0.40 w/b ratio and 0.55 w/b ratio. Especially at a 0.55 w/b ratio, due to the high amount of voids, the decrease in compressive strength and mass is higher. At 28 days of curing of 0.40 w/b ratio and 0.55 w/b ratio, we can see an increase in compressive strength and mass, suggesting that there is an ingress of water with salts into the pores of the paste matrix. However, salts do not affect the paste matrix (i.e., the formation of gypsum and ettringite has not begun yet). There is no significant change in  $\text{CaSiO}_3$  only mix W15 with respect to control mix in all w/b ratios and curing ages.

### 3.9. Field Emission Scanning Electron Microscopy (FESEM):

FESEM analysis of the paste mixes was performed to study the influence of  $\text{CaSiO}_3$  and  $\text{n-SiO}_2$  on the surface morphology of the hydrated cement matrix. At 90 days, unreacted  $\text{n-SiO}_2$  was found in NS4.5, and NS6 paste mixes indicating stoppage of the hydration process due to the unavailability of lime (Figure 9a). The  $\text{n-SiO}_2$  was found filling the voids. At 0.40 and 0.55 w/b ratios, micro-sized pores were observed in the paste mixes (Figure 9b). CSH gel formations were found in almost all the paste mixes at 28 and 90 days, and the dense CSH formations were found in NS1.5 and NS3 paste mixes (Figure 9c and 9d). The  $\text{n-SiO}_2$  formed a very dense CSH gel, increasing the mechanical strength, and it filled the voids, which will keep forming CSH gel filling the voids and increasing the mechanical properties (Figure 9d).

We also observed the  $\text{CaSiO}_3$  microfibrils reinforcing microvoids and cracks, and  $\text{n-SiO}_2$  was found filling the voids of the cement matrix (Figure 9a and 9c). In control mix, presence of calcium oxide and ettringite was determined by EDS after 28 days curing (Figure 9e). The formation of stratlingite (CASH) was observed, which happens when belite reacts with aluminium hydroxide (AH) in the presence of water (Figure 9f) (54). The chemical equation is as given in Equation [6]. This chemical reaction only takes place in the absence of CH.



Stratlingite and CSH are the primary hydration products of blended cement. Stratlingite usually

forms in blended cement as in a control cement matrix; there is always a presence of CH (55).

## 4. CONCLUSIONS

Analyzing the experimental results with the parameters and replacement levels mentioned earlier, the authors have drawn the following conclusions from the above discussions:

- I. Based on the mechanical strength results, NS3 gave the highest strength for 0.25 and 0.40 w/b ratios at both the curing ages. For a 0.55 w/b ratio, NS1.5 showed the highest value at 90 days and NS3 at 28 days. The micrograph images of NS3 showed a dense CSH gel and stratlingite formation with voids filled with  $\text{CaSiO}_3$  and  $\text{n-SiO}_2$ .
- II. Regression analysis for the mechanical properties yielded individual models for all the properties and showed the robustness and significance of the data.
- III. Sorptivity, water absorption and volume of permeable pores results indicate NS3 has a highly dense and least porous matrix in all curing ages and w/b ratios, thereby having high mechanical and durability properties. The paste mix with  $\text{CaSiO}_3$  alone (W15) shows higher porosity than the control mix due to the fibrous nature of  $\text{CaSiO}_3$ .
- IV. Sulphate treatment test was performed, and 28 days' results yielded a negligible effect on the specimen's change in strength and mass. At 90 days, the lowest change in mass and compressive strength was observed in NS1.5 and the highest in the control mix in all curing ages and w/b ratios.
- V. Micrograph images show different hydration products and nano-scale physiology of the cement matrix. The unreacted  $\text{n-SiO}_2$  in voids and bridging of pores by  $\text{CaSiO}_3$  were found with the help of FESEM. The blended cement matrix also found hydration products such as CSH gel and CASH. At a higher w/b ratio (0.55), tiny pores (7-25  $\mu\text{m}$ ) were observed at small intervals.

## ACKNOWLEDGEMENTS

We would like to gratefully acknowledge Nuoryon India Ltd, Wolkem India Ltd, and Fosroc India Pvt Ltd for providing Colloidal nanosilica, wollastonite, and Superplasticizer, respectively.

## AUTHOR CONTRIBUTIONS:

Conceptualization: T.S. Viswanathan. Data curation: N.A. Nair. Formal analysis: N.A. Nair. Funding acquisition: T.S. Viswana-

than. Investigation: T.S. Viswanathan, N.A. Nair. Methodology: N.A. Nair. Resources: T.S. Viswanathan, N.A. Nair. Software: N.A. Nair. Supervision: T.S. Viswanathan. Validation: T.S. Viswanathan. Visualization: T.S. Viswanathan, N.A. Nair. Writing, original draft: N.A. Nair. Writing, review and editing: T.S. Viswanathan, N.A. Nair

## REFERENCES

1. Kalla, P.; Rana, A.; Chad, Y.B.; Misra, A.; Csetenyi, L. (2015) Durability studies on concrete containing wollastonite. *J. Clean. Prod.* 87, 726–734. <https://doi.org/10.1016/j.jclepro.2014.10.038>.
2. Yang, K.H.; Jung, Y.B.; Cho, M.S.; Tae, S.H. (2015) Effect of supplementary cementitious materials on reduction of CO<sub>2</sub> emissions from concrete. *J. Clean. Prod.* 103, 774–783. <https://doi.org/10.1016/j.jclepro.2014.03.018>.
3. Kalla, P.; Misra, A.; Gupta, R.C.; Csetenyi, L.; Gahlot, V.; Arora, A. (2013) Mechanical and durability studies on concrete containing wollastonite-fly ash combination. *Constr. Build. Mater.* 40, 1142–1150. <https://doi.org/10.1016/j.conbuildmat.2012.09.102>.
4. Nair, N.A.; Sairam, V. (2021) Research initiatives on the influence of wollastonite in cement-based construction material- A review. *J. Clean. Prod.* 283, 124665. <https://doi.org/10.1016/j.jclepro.2020.124665>.
5. Ransinching, G.D.; Kumar, B. (2010) Investigations on pastes and mortars of ordinary portland cement admixed with wollastonite and microsilica. *J. Mater. Civ. Eng.* 22, 305–313. [https://doi.org/10.1061/\(ASCE\)MT.1943-5533.0000019](https://doi.org/10.1061/(ASCE)MT.1943-5533.0000019).
6. Soliman, A.M.; Nehdi, M.L. (2012) Effect of natural wollastonite microfibers on early-age behavior of UHPC. *J. Mater. Civ. Eng.* 24, 816–824. [https://doi.org/10.1061/\(ASCE\)MT.1943-5533.0000473](https://doi.org/10.1061/(ASCE)MT.1943-5533.0000473).
7. Abhilash, P.P.; Nayak, D.K.; Sangoju, B.; Kumar, R.; Kumar, V. (2021) Effect of nano-silica in concrete; a review. *Constr. Build. Mater.* 278, 122347. <https://doi.org/10.1016/j.conbuildmat.2021.122347>.
8. Sobolev, K.; Gutiérrez, M.F. (2005) How nanotechnology can change the concrete world. *Am. Ceram. Soc. Bull.* 84, 14–18. <https://doi.org/10.1002/9780470588260.ch16>.
9. Niu, Y.M.; Zhu, X.L.; Chang, B.; Tong, Z.H.; Cao, W.; Qiao, P.H.; Zhang, Lin-Yuan; Zhao, J.; Song, Y.G. (2016) Nanosilica and Polyacrylate/Nanosilica: A Comparative Study of Acute Toxicity. *BioMed Res. Int.* 2016, 1–7. <https://doi.org/10.1155/2016/9353275>.
10. Jo, B.W.; Kim, C.H.; Lim, J.H. (2007) Investigations on the development of powder concrete with nano-SiO<sub>2</sub> particles. *KSCE J. Civ. Eng.* 11, 37–42. <https://doi.org/10.1007/bf02823370>.
11. Sharma, S.K. (2019) Properties of SCC containing pozzolans, Wollastonite micro fiber, and recycled aggregates. *Heliyon* 5, 1–12. <https://doi.org/10.1016/j.heliyon.2019.e02081>.
12. Peris Mora, E. (2007) Life cycle, sustainability and the transcendent quality of building materials. *Build. Environ.* 42 [3], 1329–1334. <https://doi.org/10.1016/j.buildenv.2005.11.004>.
13. Huang, H.; Guo, R.; Wang, T.; Hu, X.; Garcia, S.; Fang, M.; Luo, Z.; Maroto-Valer, M.M. (2019) Carbonation curing for wollastonite-Portland cementitious materials: CO<sub>2</sub> sequestration potential and feasibility assessment. *J. Clean. Prod.* 211, 830–841. <https://doi.org/10.1016/j.jclepro.2018.11.215>.
14. Low, N.M.P.; Beaudoin, J.J. (1993) The effect of wollastonite micro-fibre aspect ratio on reinforcement of Portland cement-based binders. *Cem. Concr. Res.* 23 [6], 1467–1479. [https://doi.org/10.1016/0008-8846\(93\)90083-L](https://doi.org/10.1016/0008-8846(93)90083-L).
15. Low, N.M.P.; Beaudoin, J.J. (1994) Mechanical properties and microstructure of high alumina cement-based binders reinforced with natural wollastonite micro-fibres. *Cem. Concr. Res.* 24 [4], 650–660. [https://doi.org/10.1016/0008-8846\(94\)90189-9](https://doi.org/10.1016/0008-8846(94)90189-9).
16. Low, N.M.P.; Beaudoin, J.J. (1994) The flexural toughness and ductility of portland cement-based binders reinforced with wollastonite micro-fibres. *Cem. Concr. Res.* 24 [2], 250–258. [https://doi.org/10.1016/0008-8846\(94\)90050-7](https://doi.org/10.1016/0008-8846(94)90050-7).
17. Sobolev, K.; Flores, I.; Hermsillo, R.; Torres-Martínez, L.M. (2008) Nanomaterials and nanotechnology for high-performance cement composites. *Am. Concr. Institute, ACI Spec. Publ.* SP-254, 91–118. <https://doi.org/10.14359/20213>.
18. Heidari, A.; Tavakoli, D. (2013) A study of the mechanical properties of ground ceramic powder concrete incorporating nano-SiO<sub>2</sub> particles. *Constr. Build. Mater.* 38, 255–264. <https://doi.org/10.1016/j.conbuildmat.2012.07.110>.
19. Aggarwal, Y.; Siddique, R. (2014) Microstructure and properties of concrete using bottom ash and waste foundry sand as partial replacement of fine aggregates. *Constr. Build. Mater.* 54, 210–223. <https://doi.org/10.1016/j.conbuildmat.2013.12.051>.
20. Ji, T. (2005) Preliminary study on the water permeability and microstructure of concrete incorporating nano-SiO<sub>2</sub>. *Cem. Concr. Res.* 35 [10], 1943–1947. <https://doi.org/10.1016/j.cemconres.2005.07.004>.
21. Said, A.M.; Zeidan, M.S.; Bassuoni, M.T.; Tian, Y. (2012) Properties of concrete incorporating nano-silica. *Constr. Build. Mater.* 36, 838–844. <https://doi.org/10.1016/j.conbuildmat.2012.06.044>.
22. Naji Givi, A.; Abdul Rashid, S.; Aziz, F.N.A.; Salleh, M.A.M. (2010) Experimental investigation of the size effects of SiO<sub>2</sub> nano-particles on the mechanical properties of binary blended concrete. *Compos. Part B: Eng.* 41 [8], 673–677. <https://doi.org/10.1016/j.compositesb.2010.08.003>.
23. ASTM C618-19 (2019) Standard specification for coal fly ash and raw or calcined natural pozzolan for use in concrete. *Annu. B. ASTM Stand.* 2019, 1-4. <https://doi.org/10.1520/C0618-19>.
24. IS 12269 (2013) Ordinary portland cement — 53 grade specification, *Indian Stand.* 2013, 1-14.
25. ASTM C305 (2014) Standard practice for mechanical mixing of hydraulic cement pastes and mortars of plastic consistency. *Annu. B. ASTM Stand.* 2014, 1-3.
26. Bolhassani, M.; Samani, M. (2015) Effect of type, size, and dosage of nanosilica and microsilica on properties of cement paste and mortar. *ACI Mater. J.* 112, 259–266. <https://doi.org/10.14359/51686995>.
27. IS 516- Part 11 (2020) Hardened concrete — methods of test. *Indian Stand.* 2020, 1-8.
28. Hall, C. (1989) Water sorptivity of mortars and concretes: a review. *Mag. Concr. Res.* 41 [147], 51–61. <https://doi.org/10.1680/macr.1989.41.147.51>.
29. ASTM C1585 (2013) Standard test method for measurement of rate of absorption of water by hydraulic cement concretes. *Annu. B. ASTM Stand.* 41, 1–6.
30. Larbi, J.A. (1993) Microstructure of the interracial zone around aggregate particles in concrete. *Heron* 38, 1–69. Retrieved from <https://heronjournal.nl/38-1/1.pdf>.
31. Neville, A. (2004) The confused world of sulfate attack on concrete. *Cem. Concr. Res.* 34 [8], 1275–1296. <https://doi.org/10.1016/j.cemconres.2004.04.004>.
32. Clifton, J.R.; Frohnsdorff, G.; Ferraris, C. (1998) Standards for evaluating susceptibility of cement based materials to External Sulphate Attack. *Am. Ceram. Soc. Special Volume*, 337–355. Retrieved from [https://tsapps.nist.gov/publication/get\\_pdf.cfm?pub\\_id=860169](https://tsapps.nist.gov/publication/get_pdf.cfm?pub_id=860169)
33. Thaulow, N.; Sahu, S. (2004) Mechanism of concrete deterioration due to salt crystallization. *Mat. Charact.* 53, 123–127. <https://doi.org/10.1016/j.matchar.2004.08.013>.
34. Min, D.; Mingshu, T. (1994) Formation and expansion of ettringite crystals. *Cem. Concr. Res.* 24 [1], 119–126. [https://doi.org/10.1016/0008-8846\(94\)90092-2](https://doi.org/10.1016/0008-8846(94)90092-2).
35. Fathima Suma, M.; Santhanam, M.; Rahul, A. V. (2020) The effect of specimen size on deterioration due to external sodium sulphate attack in full immersion studies. *Cem. Concr. Compos.* 114, 103806. <https://doi.org/10.1016/j.cemconcomp.2020.103806>.
36. Mehta, P.K. (1976) Scanning electron micrographic studies of ettringite formation. *Cem. Concr. Res.* 6 [2], 169–182. [https://doi.org/10.1016/0008-8846\(76\)90115-0](https://doi.org/10.1016/0008-8846(76)90115-0).
37. Sharma, U.; Singh, L.P.; Ali, D.; Poon, C.S. (2019) Effect of particle size of silica nanoparticles on hydration reactivity and microstructure of C-S-H gel. *Adv. Civ. Eng. Mater.* 8, 346–360. <https://doi.org/10.1520/acem20190007>.

38. Hewlett, P.C. (2004) *Lea's chemistry of cement and concrete*. 2<sup>nd</sup> ed., Elsevier Science & Technology Books, Amsterdam, (2004).
39. Chithra, S.; Senthil Kumar, S.R.R.; Chinnaraju, K. (2016) The effect of colloidal nano-silica on workability, mechanical and durability properties of high performance concrete with copper slag as partial fine aggregate. *Constr. Build. Mater.* 113, 794–804. <https://doi.org/10.1016/j.conbuildmat.2016.03.119>.
40. Neville, A.M.; Brooks J.J. (2010) *Concrete technology*. Pearson education limited, Essex, (2010).
41. Bentz, D.P.; Sant, G.; Weiss, J. (2008) Early-age properties of cement-based materials. I: influence of cement fineness. *J. Mater. Civ. Eng.* 20, 502–508. [https://doi.org/10.1061/\(asce\)0899-1561\(2008\)20:7\(502\)](https://doi.org/10.1061/(asce)0899-1561(2008)20:7(502)).
42. Levasil, C.B. (2019) Strong constructions that last saving resources by improving performance. Nouryon Ltd., Sweden, (2019).
43. Montgomery, D.C. (2001) *Design and analysis of experiments*. 5 ed., John Wiley & Sons, Inc. New York, (2001).
44. Rahimzadeh, C.Y.; Salih, A.; Barzinjy, A.A. (2022) Systematic multiscale models to predict the compressive strength of cement paste as a function of microsilica and nanosilica contents, water/cement ratio, and curing ages. *Sustain.* 14 [3], 1–23. <https://doi.org/10.3390/su14031723>.
45. Dahasahastra, A.V.; Balasundaram, K.; Latkar, M.V. (2022) Hydrometallurgy Turbidity removal from synthetic turbid water using coagulant recovered from water treatment sludge: A potential method to recycle and conserve aluminium. *Hydrometallurgy.* 213, 105939. <https://doi.org/10.1016/j.hydromet.2022.105939>.
46. Mohammed, A.; Mahmood, W.; Ghafor, K. (2020) TGA, rheological properties with maximum shear stress and compressive strength of cement-based grout modified with polycarboxylate polymers. *Constr. Build. Mater.* 235, 117534. <https://doi.org/10.1016/j.conbuildmat.2019.117534>.
47. Zain, M.F.M.; Abd, S.M. (2009) Multiple regression model for compressive strength prediction of high performance concrete. *J. App. Sci.* 9 [1], 155–160. <https://doi.org/10.3923/jas.2009.155.160>.
48. Neville, A.M. (2011) *Properties of concrete*. 5th Ed., Pearson Education Limited, England, (2011).
49. ASTM C642 (2013) Standard test method for density, absorption, and voids in hardened concrete. *Annu. B. ASTM Stand.* 2013, 1-3.
50. Jindal, A.; Ransinchung R.N., G.D.; Kumar, P. (2019) Behavioral study of self-compacting concrete with wollastonite microfiber as part replacement of sand for pavement quality concrete (PQC). *Int. J. Transp. Sci. Technol.* 9 [2], 170–181. <https://doi.org/10.1016/j.ijst.2019.06.002>.
51. Sakai, E.; Kasuga, T.; Sugiyama, T.; Asaga, K.; Daimon, M. (2006) Influence of superplasticizers on the hydration of cement and the pore structure of hardened cement. *Cem. Concr. Res.* 36 [11], 2049–2053. <https://doi.org/10.1016/j.cemconres.2006.08.003>.
52. Du, H.; Pang, S.D. (2019) High performance cement composites with colloidal nano-silica. *Constr. Build. Mater.* 224, 317–325. <https://doi.org/10.1016/j.conbuildmat.2019.07.045>.
53. Yang, L.; Gao, D.; Zhang, Y.; Tang, J.; Li, Y. (2019) Relationship between sorptivity and capillary coefficient for water absorption of cement-based materials: Theory analysis and experiment. *R. Soc. Open Sci.* 6, 1-12. <https://doi.org/10.1098/rsos.190112>.
54. Pimraksa, K.; Chindaprasirt, P. (2018) Sulfoaluminate cement-based concrete. *Eco-efficient Repair Rehabil. Concr. Infrastruc.* 1, 355-385 <https://doi.org/10.1016/B978-0-08-102181-1.00014-9>.
55. Yuan, Q.; Liu, Z.; Zheng, K.; Ma, C. (2021) *Civil Engineering Materials*. 1<sup>st</sup> Ed., Woodhead Publishing Series, Cambridge, (2021).